Microbubble PhoXonic Resonators: chaos transition and transfer

Xavier Rosello–Mecho[a], Gabriele Frigenti[b,c], Daniele Farnesi[b], Martina Delgado-Pinar[a], Miguel V. Andrés[a], Fulvio Ratto[b], Gualtiero Nunzi Conti[b], Silvia Soria[b]

[a] *Departamento de Fisica Aplicada - ICMUV, Universidad de Valencia, Dr. Moliner 50, Burjasot, 46100, Valencia, Spain*
[b] *CNR-IFAC Institute of Applied Physics "N.Carrara", Via Madonna del Piano 10, Sesto Fiorentino, 50019, Florence, Italy*
[c] *Laboratorio Europeo di Spettroscopia Nonlineare (LENS) - Università degli Studi di Firenze, Via Nello Carrara 1, Sesto Fiorentino, 50019, Florence, Italy*

Abstract

We report the activation of optomechanical chaotic oscillations in microbubble resonators (MBRs) through a blue-side excitation of its optical resonances. We confirm the sequence of quasi-periodical oscillation, spectral continuum and aperiodic motion; as well as the transition to chaos without external feedback or modulation of the laser source. In particular, quasi periodic transitions and a spectral continuum are reported for MBRs with diameters up to 600 µm, whereas only an abrupt transition into a spectral continuum is observed for larger microbubbles.

Keywords: whispering gallery modes, chaos, resonators, optomechanical oscillators, chaos transfer
PACS: 0000, 1111
2000 MSC: 0000, 1111

1. Introduction

Whispering gallery mode resonators are a family of optical resonators capable of trapping light on a circular path through the combination of their cylindrical symmetry and of total internal refraction. The optical mode so formed is called Whispering Gallery Mode (WGM) and takes its name from the analogous acoustic phenomena studied by Lord Rayleigh under the dome

of the Saint Paul cathedral in London. The most straightforward Whispering gallery mode resonator (WGMR) is the microsphere, but several other geometries can be produced, such as microdisks, microtoroids, microrings or micropillars. Regardless of the specific geometry, all WGMRs have a rich spectrum of sharp optical resonances (with the sharpness being quantified through the quality factor Q) and this feature is the key element for their implementation in various applications. For example, the sharpness of the resonances allows the WGMRs to be sensitive optical sensors, precise optical filters or high finesse micro-cavities for lasing or the generation of non-linear effects. A special type of WGMRs are the hollow ones, which are fabricated by heating a pressurized glass capillary [1, 2], mimicking the fabrication prowess of the glassblowers on the micro-scale. In the case of a spherical bulge, these resonators are called microbubble resonators (MBRs); while in the case of an ellipsoidal bulge, they are called microbottle resonators.

In this article, we focus on the opto-mechanical properties of the microbubble resonators , which are the last arrived in the WGMR family [3]. It has been demonstrated that MBRs can be used to study Turing comb patterns (Kerr modulation) and Stimulated Brillouin Scattering (SBS) [4, 5, 6, 7, 8], proving their ability in sustaining not only the photons running in their optical modes, but also the phonons of the material making up the MBR. To highlight this double possibility, MBRs are also labelled as phoXonic cavities, combining the words "photon" and "phonon" in a single term. In addition of phonons, MBRs can also sustain lower frequency mechanical modes featuring an overall vibration, expansion or bending of the MBR walls. As in the optical case, these mechanical modes make up a sharp and dense spectrum and consequently make MBRs efficient mechanical resonators.

As shown in the pioneering work of Kippenberg et al. on microtoroids [10], these modes can be excited through the radiation pressure (RP) produced by the photons running in the optical modes [11] and this leads to an interesting interplay between the optical and the mechanical modes of the resonator. In a nutshell, the interaction between an optical mode (frequency ω_R) and a mechanical mode (frequency Ω_m) in a WGMR can be resumed as follows [12, 13].

A slightly detuned laser source (frequency ω_L) is used to excite the WGM and produce a high circulating optical power. Due to the high power, the radiation pressure activates the mechanical mode, producing a sinusoidal perturbation of the resonator optical length with frequency Ω_m. In analogy with phase modulators, this oscillation produces two sidebands waves inside

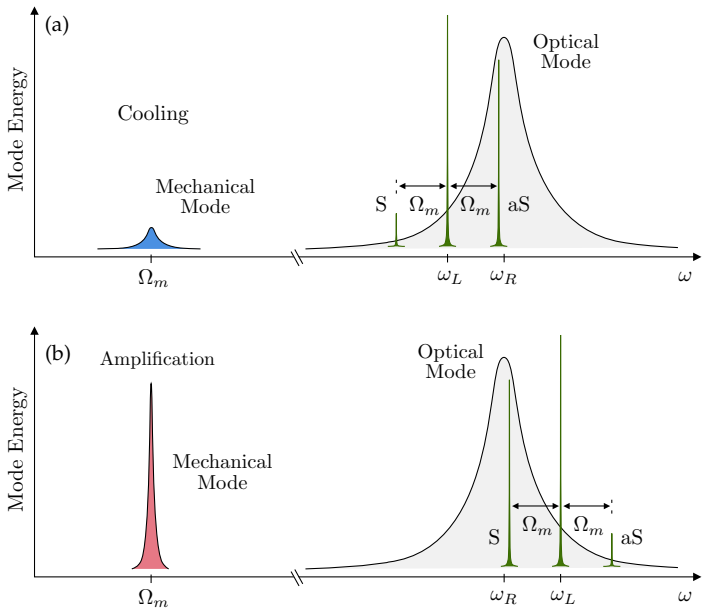

Figure 1: Graphical description of the activation of opto-mechanical oscillations, based on the resonance of the Stokes or anti-Stokes sidebands [9].

of the resonator at frequencies $\omega_L - \Omega_m$ (Stokes band) and $\omega_L + \Omega_m$ (anti-Stokes band). If one of the sidebands is perfectly resonant with the WGM (i.e. if $\omega_L - \Omega_m = \omega_R$ or $\omega_L + \Omega_m = \omega_R$; see Figure 1), the sideband wave is guided by the WGM and its interaction with the laser wave is enhanced because of the high finesse of the resonator (i.e. long photon lifetimes increase the interaction time). Depending on the laser source detuning, the interaction can lead to positive or negative feedback, and therefore amplify or quench the mechanical mode.

If the laser source is red-detuned ($\omega_L < \omega_R$), the anti-Stokes band is resonant and, in terms of optical energy, the best configuration is achieved by moving the energy on the laser wave. This, in turn, produces the depletion of the sideband wave and also the removal of some energy from the mechanical mode. Since the mechanical mode loses energy in this configuration (negative feedback), one talks of *negative RP back-action*. If, instead, the laser source is blue-detuned ($\omega_L > \omega_R$), the Stokes band is resonant and therefore the best configuration is achieved by moving the energy on the sideband wave. This, in turn, enhances the sideband amplitude and increases the energy in the mechanical mode (positive feedback). In this configuration, one talks of

positive RP back-action.

Both negative and positive RP back-action is interesting for scientific research. Negative back-action, in fact, can be used to suppress thermal oscillations and therefore move the mechanical oscillator towards a quantum regime. Positive back-action, instead, can lead to clearly measurable optomechanical oscillations (OMOs) in WGMRs [14]. In this second case, which is the one of interest for this article, the OMOs are triggered by launching sufficient power into the WGMRs and are read through the shift induced into the optical resonance. In particular, the position of the resonance oscillates at the frequency of the mechanical mode (Ω_M) and this causes a modulation of the WGMR at the same frequency.

After the pioneering work in toroids [15, 10, 16], the optomechanical oscillations have been observed in other WGMRs, such as spheroids [17], solid microbottles [18] and MBRs [19]. In addition, OMOs were also found in combination with nonlinear optical effects (NLOE): in particular, since OMOs activation threshold is typically lower, NLOEs typically start when the cavity is already oscillating. This coexistence, however, is not in general guaranteed: the two processes, in fact, compete on activation [20, 19] and configurations where one is enhanced at the expense of the other are possible. Finally, it was shown [16] that launching high input powers into toroids and spheroids produces an erratic behaviour, which is experimentally observed through the formation of period doubling [17]. A decade after this initial study, chaos mediated stochastic resonance and chaos transfer in a toroid were also demonstrated [21]. Despite of the interest in the temporal behavior of nonlinearities in WGMRs, the optomechanical chaotic behavior has remained largely unexplored experimentally and the study here presented aims at filling this gap for the MBR system.

Here we report the activation of OMOs in MBRs and their evolution into a chaotic behavior using a continuous wave (CW) source, without the use of external feedback, modulation, delay or periodic perturbation. We show two different routes to chaos for the MBR system and also a chaos transfer between an high-power pump WGM exciting the OMO and a low-power probe WGM within the same MBR. In analogy with toroids, the increase of pump power produced the same route to chaos for both the pump and the probe WGMs. Indeed, the results here presented show that RP induced chaotic motion is not limited to a special kind of WGMR, but it is an intrinsic property of the optical cavity [17].

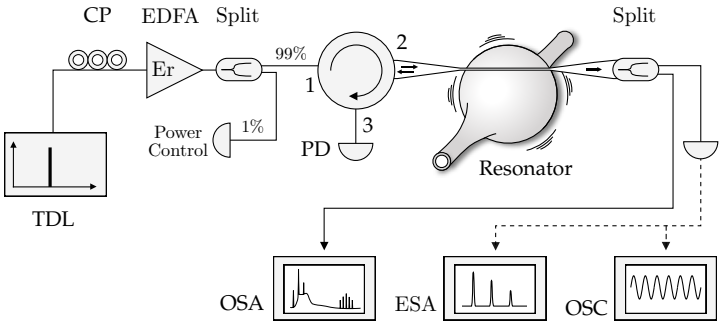

Figure 2: Scheme of the experimental setup employed to excite and measure the optomechanical vibrations induced by RP [9]. The following abbreviations are used: TDL: tunable laser diode, CP: polarisation controller, EDFA: erbium doped fiber amplifier, Split: fiber coupler (in this case used as a splitter), OSA: optical spectrum analyser, ESA: electrical spectrum analyser, OSC: oscilloscope, PD: photodiode.

2. Experimental setup

The experimental setup used to trigger and characterise the opto-mechanical oscillations of a MBR is shown in Figure 2. In this setup, the emission of a tunable laser source centered at 1550 nm (Nettest TUNICS-Plus) was incremented with an erbium-doped fiber amplifier (IPG Photonics) and then launched into a 2 µm home-made tapered fiber to excite the WGMs of an MBR. The transmission of the MBR was then split between an optical spectrum analyser (Ando AQ6317B, resolution: 20 pm) and a fast photodetector (Thorlabs PDA400), connected either to an oscilloscope (Tektronix DPO7104), or to an electrical spectrum analyser (Rohde & Schwarz FSL, 9 kHz-6 GHz). To measure the optical power exciting the MBR, a small fraction of the launched power was monitored with a power meter (Ando AQ2140).

For this experiment, the MBRs were fabricated using an electrical arc discharge technique [1] and exhibited diameters ranging from 420 to 780 µm and wall thicknesses ranging from 2 to 6 µm.. In particular, the wall thicknesses were estimated through a model based on the conservation of mass during the glassblowing phase and accounting for both capillary size and bubble diameter [22].

The experiment was split into two parts. In the first part, we measured the WGM resonances by scanning the laser wavelength at low input power, to be sure that nonlinear phenomena were below their threshold, and that thermal broadening/narrowing of the resonance was negligible. From these

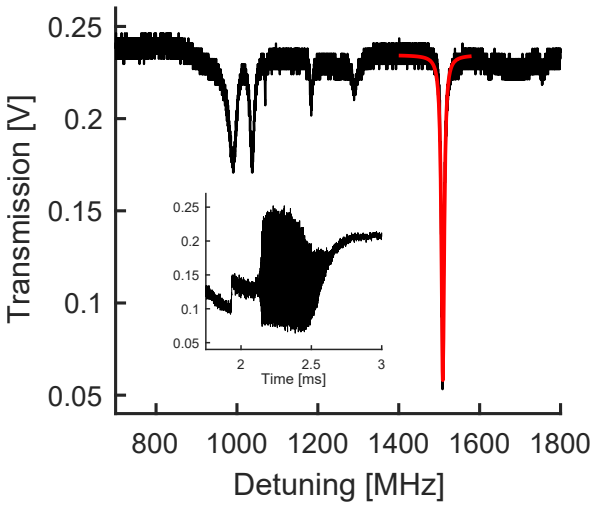

Figure 3: Typical optical transmission below threshold. Inset: high power thermally induce line broadening and mechanical oscillations

initial measurements it was possible to estimate the quality factor Q of the resonances, finding values ranging from 10^6 to 10^7 (see Figure 3). Then, we moved to the second part of the experiment, where OMOs and nonlinear phenomena were triggered. In particular, we started by identifying resonances showing passive thermal locking during the wavelength scan [23] and then increased the input power. Since thermal locking allowed the laser to stay blue-detuned with the resonance and increase the energy build-up into the resonator, this method allowed to exceed the activation threshold of OMOs and/or of other non-linear phenomena. The inset of Figure 3 shows the OMO activation (central part) as well as the deformation of the Lorentzian shape due to thermal locking (left part). In the following Sections, signals like these are analyzed in detail to investigate the opto-mechanical properties of the MBR.

3. Features of the optomechanical oscillation

As discussed in the previous Section, thermal locking allows to lock the laser source to the blue-side of a WGM resonance, and, if the input power exceeds the activation threshold [19], the mechanical modes of the MBR can be excited. In particular, below threshold, the MBR signal remains constant, as it corresponds to a locked resonance. Above threshold, instead, the MBR

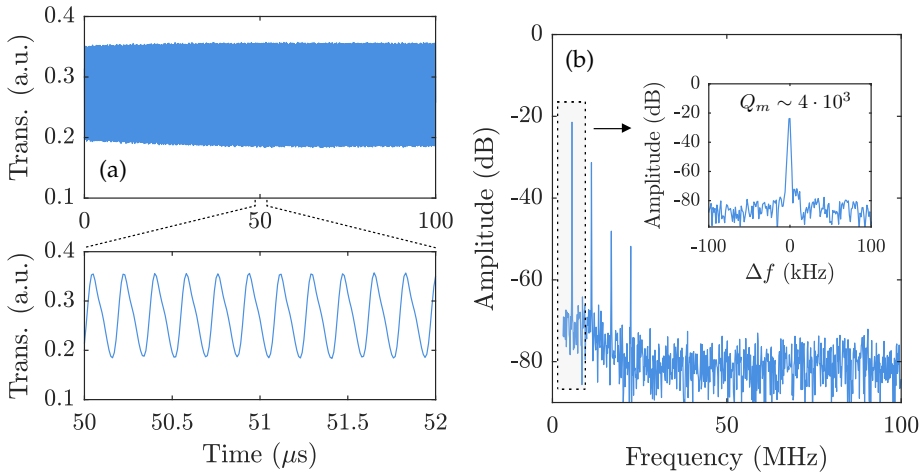

Figure 4: a) Harmonic modulation of the system transmittance due to the optomechanical vibration. b) Frequency vibration and mechanical Q-factor

signal shows a clear quasi-harmonic oscillation, as shown in Figure 4 for an input power of 200 mW. More specifically, Figure 4a shows the MBR transmission as measured by the oscilloscope, while Figure 4b shows the same signal measured through the electric spectrum analyzer (cfr. Figure 2) . The ESA measurement shows a narrow peak at 5.63 MHz, corresponding to the eigenfrequency of a fundamental vibrational mode, and then a series of less intense peaks, corresponding to various harmonics. The inset of Figure 4b shows a magnification of the area around the principal peak, highlighting that this mode had a mechanical Q factor close to $4 \cdot 10^3$. To estimate the temporal stability of the mechanical vibration, we monitored the ESA signal for more than 3 minutes, finding amplitude variations of the fundamental peak below 1.5 dB and position variations within 1.3 kHz [19].

After these measurements, we studied the evolution of the fundamental peak amplitude as a function of the input power. Figure 5a clearly shows an oscillation threshold at about 40 mW, followed by a gain saturation at about 140mW. We explain the saturation effect as a consequence of the shape of the WGM resonance. In particular, for lower input powers, the WGM resonance oscillates within its full-width half maximum, making the laser probe only the linear edge of the resonance. Instead, for higher input powers, the resonance moves beyond its full-width half maximum, making the laser probe also the curved zone around the minimum (see Figure 5b). This curved shape is

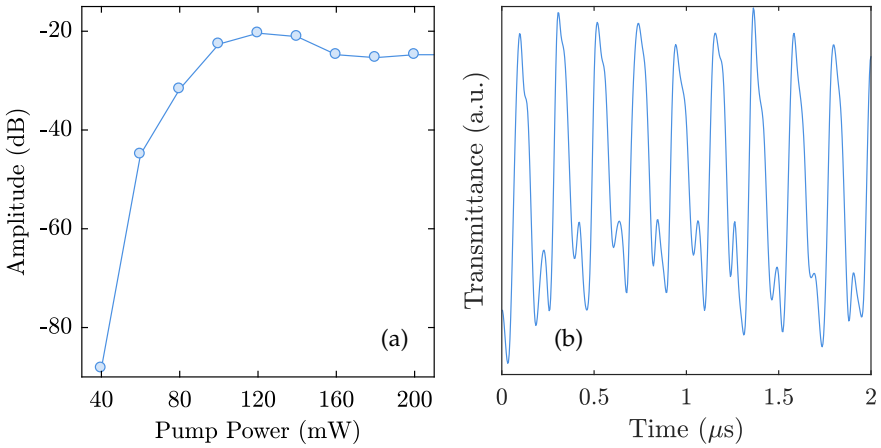

Figure 5: a) Evolution of the fundamental peak amplitude as a function of the pump power. b) Distortion of the transmittance modulation due to the resonance shape

indeed nonlinear and can produce higher order harmonics in the ESA.

To further verify that the modulation observed in the optical signal was due to a mechanical mode of the MBR, we repeated the experiment with a pump-and-probe approach. In this configuration, we excited simultaneously two counter-propagating WGMs at different wavelengths using two laser sources. In particular, one WGM was excited as shown so far, using the amplified 1550 nm source (pump laser) to trigger the opto-mechanical oscillations. The other WGM, instead, was excited using a low power 1480 nm source (Anritsu TUNICS-Reference, probe laser) and was used to interrogate the system. The results of the pump-and-probe test are shown in Figure 6, where both the raw WGMs transmissions and their respective ESA measurements are plotted. Indeed, the ESA plots clearly show that the mechanical modulation induced by the pump WGM at 1550 nm was transferred to the probe WGM at 1480 nm. In practical terms, this transfer is the consequence of the probe WGM reading the perturbations of the MBR refractive index and the MBR radius induced by the mechanical vibrations. Other explanations are excluded, since the WGMs were distant in wavelength and therefore no direct cross-talk was possible; and since the probe source was very low in power (around 1 mW) and therefore it could not trigger the oscillation. In more general terms, oscillation transfer can represent an interesting method to indirectly couple two WGMs, taking advantage on a mechanical mode

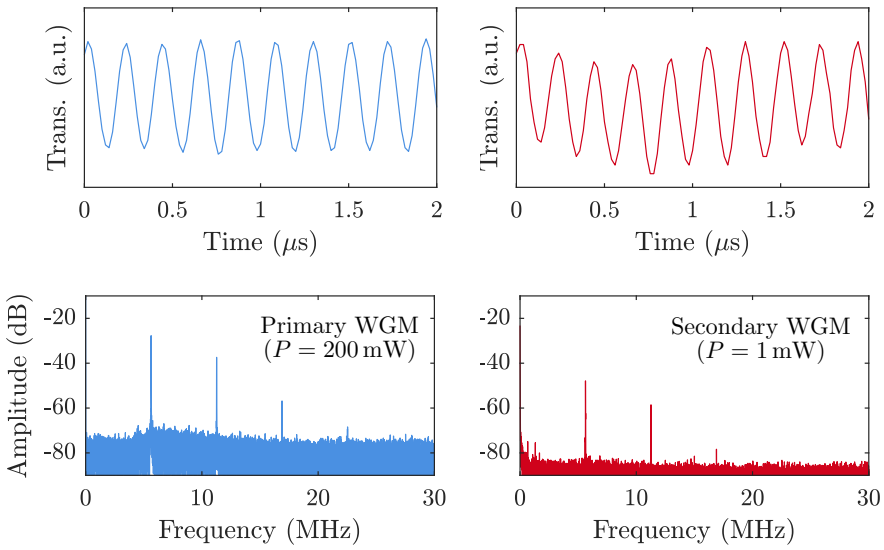

Figure 6: Pump and probe measurement of the transmittance modulation induced by the primary WGM (P= 200 mW)

having a significant overlap with two WGMs distributions.

During the pump-and-probe experiment, we also observed optical nonlinear effects such as Four Wave Mixing (FWM), Stimulated Raman Scattering (SRS) and Stimulated Brillouin Scattering (SBS) simultaneously to the optomechanical vibrations (see Figure 7A and 7B for the case of SBS). Since nonlinear optical effects and OMOs are competitive processes [20, 19], the coexistence of the two types of processes was sensitive towards the conditions of thermal locking. For certain locking conditions at high launched optical power, in fact, we observed an amplification of the vibrations and a suppression of the optical nonlinearities. Finally, Figure 7c shows that the power of the probe source was low enough to avoid the activation of optical nonlinearities, as well as OMOs.

We studied the activation of OMOs for MBRs of different sizes [19], with Figure 8 showing the measured vibrational frequencies as a function of the MBR diameter. We identified two different ranges for the vibrational frequencies: a high frequency range (order of MHz) for MBRs below 600 µm, and a low frequency range (hundreds of kHz) for larger MBRs. It can be observed that in the MHz range the vibrational frequency decreases as the MBR diameter increases, while in the kHz range the vibrational frequency is

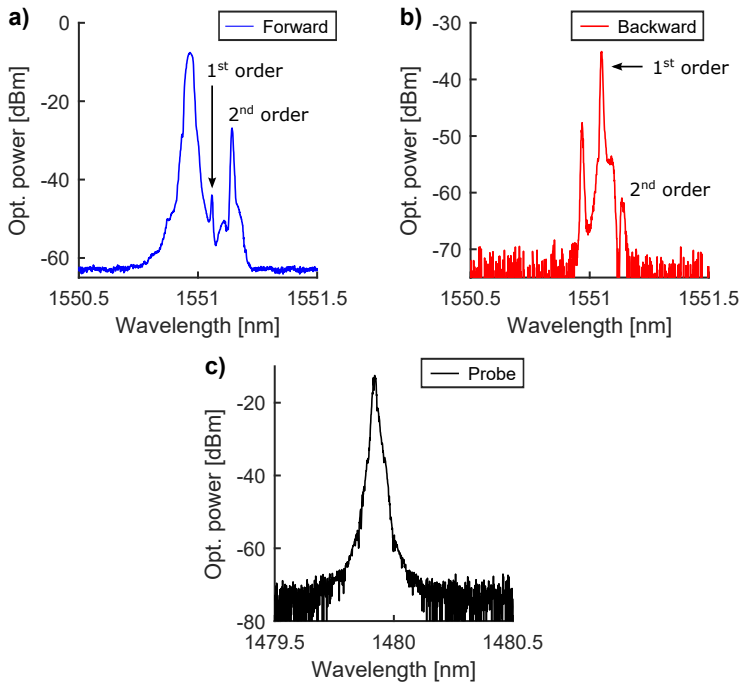

Figure 7: Spectra of Stimulated Brillouin Scattering (SBS) in the MBR: a) in forward direction by the primary WGM (P= 200 mW); b) in backward direction by the primary WGM and c) OSA signal of the secondary WGM (P= 1mW) without any nonlinear effect

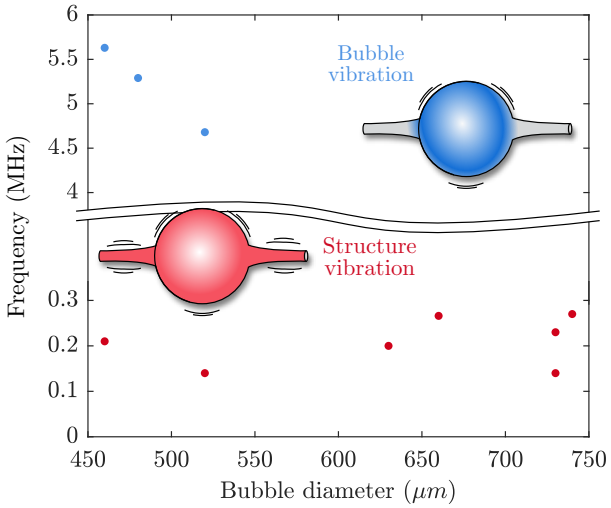

Figure 8: Experimental vibrational frequencies as a function of the MBR diameter. Illustration of the two types of vibrations that were identified in the two ranges of frequencies

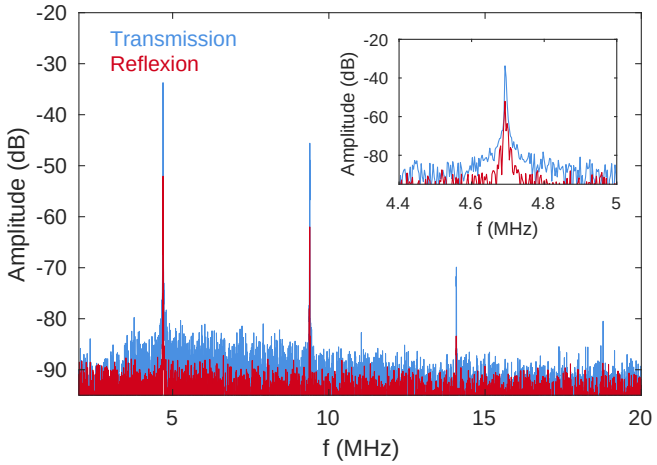

Figure 9: ESA measurement of the transmitted and reflected field. Inset: zoom of the main mechanical mode

independent from the MBR diameter. We ran numerical simulations using a commercial finite element method software (COMSOL) to obtain the theoretical vibrational eigenmodes of the MBR and identify which ones were excited in the experiment. From the these numerical results, we concluded that the MHz vibrations are mechanical modes of the MBR spherical bulge, while the kHz vibrations correspond to mechanical modes of the whole structure (i.e. the combination of both the spherical bulge and the capillary).

As a final characterization test, we also checked the presence of the optomechanical oscillations on the back-reflected WGM (see additional photodiode on the third circulator branch in Figure 2). As shown in Figure 9 through the ESA measurements, the OMOs are present in the backward direction and their spectra is identical to the one measured in the forward direction. Indeed, this forward-and-backward test, together with the previous pump-and-probe test, demonstrates that the OMOs are not only limited to the WGM triggering the oscillations, but also affect all WGMs of the microbubble.

4. Route to Chaos

The route to chaos for spheres and toroids was first reported by Carmon et al [17] and it has been recently observed by Monifi et al [21]. In all

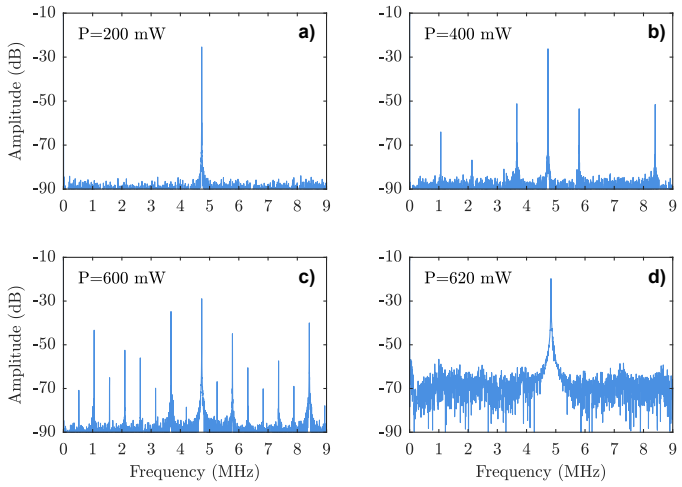

Figure 10: Transition to chaos as the launched power is increased: a) 200mW, b)400mW, c)600mW and d) 620mW.The MBR has a diameter of about 520 µm and a wall thickness of 4.26 µm. The fundamental mode is centered at 4.74 MHz

cases, the authors reported a transition to a chaotic regime through periodic-doubling bifurcation cascades [24]. Here we present, up to our knowledge, the first experimental results describing the route to chaos for MBRs. In the following, this transition is discussed for MBRs of different sizes and, in analogy with the previous Section, also using pump-and-probe approach. In these experiments we tried to maintain the same experimental conditions for all the MBRs. For example, we always excited the WGMs at the equator of the MBR, to produce similar optical field distributions between the various MBRs. Nevertheless, passive thermal locking has limits in the selection of the locked WGM resonance and also in the detuning of the locking point. Therefore, the excitation of WGMs with different radial, azimuthal and polar orders between the various experiments is possible. Indeed this fact can affect the different routes to chaotic motion for large input powers, since the activation of a certain mechanical mode depends on its overlap with the excited WGM.

We start our overview on the chaos routes by describing the behavior of an MBR having a 520 µm diameter: in particular, we focused on describing the composition of the OMOs frequencies as the input power was increased (Figure 10). For this MBR, the route began with a periodic regime with only a few sharp peaks (Figure 10b), then it moved to a quasi-periodic doubling

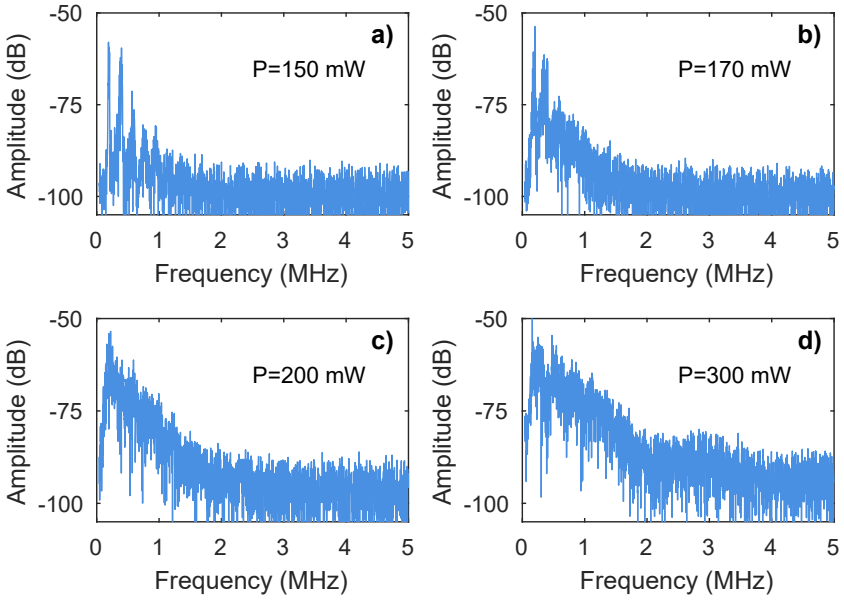

Figure 11: Transition to chaos as the launched power is increased: a) 150mW, b)170mW, c)200mW and d) 300mW. The MBR has a diameter of about 630 µm and a wall thickness of 2.90 µm. The fundamental mode is centered at 200 kHz.

regime increasing the number of discrete lines (Figure 10c), and finally ended up with a continuum of frequencies for input powers above 600 mW (Figure 10d). In particular, for this final phase, we observed an increment of the whole baseline due to the broadening and the merging of secondary peaks into the continuum, with only the fundamental frequencies and its high harmonics above it. All these results agree very well with those of previous studies [21, 17, 24].

For large MBRs (diameters above 600 µm), however, the transition to chaos was different and, in particular, an abrupt one. As shown in Figure 11, in fact, the MBR fell directly into the frequency continuum, skipping the formation of the discrete peaks associated with the quasi periodic doubling (cfr. Figure 10).

Finally, in analogy with Section 2, we also performed a pump-and-probe characterization to observe the chaos routes for both a pump WGM and a probe WGM. The frequency spectra of Figure 12 show that the two WGMs perform the same route, since the spectra differ only by scaling factors. Since the MBR has a 500 µm diameter, the chaos route features the quasi-periodic

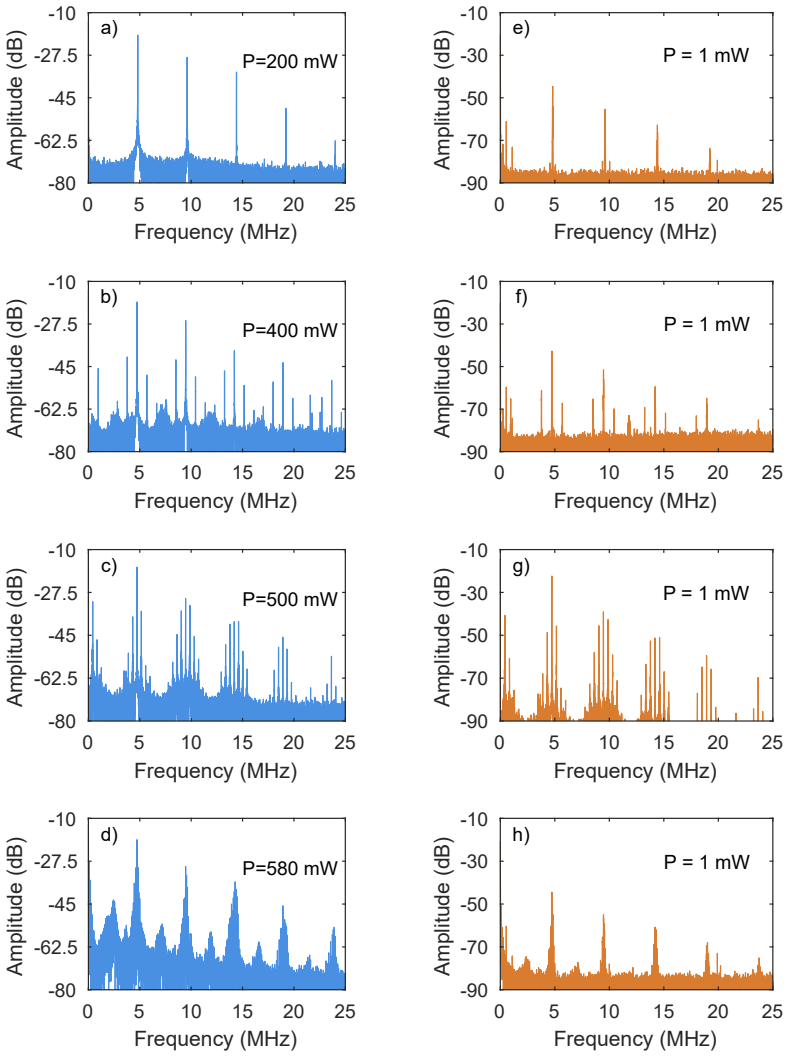

Figure 12: Transition to chaos of the pump WGM (left column) and of the probe WGM (right column) as the launched power is increased from 200mW to 620mW and the probe power is kept to 1 mW. This MBR had a diameter of about 500 µm and a wall thickness of 4.26 µm, and its fundamental mode was centered at 4.74 MHz.

doubling regime before reaching the frequency continuum. As in the previous pump-and-probe experiment, the chaotic oscillations on the probe WGMs are the read-out of the perturbations of the MBR refractive index and the MBR radius induced by the chaotic mechanical vibrations.

5. Conclusions

We presented an experimental study demonstrating radiation-pressure induced optomechanical oscillations in a microbubble resonator, and their transition to a chaotic regime. The experiment was performed at room temperature using a continuous wave source and the chaotic vibration was reached without any external feedback or modulation. We have shown that the OMOs and the chaotic regime can be reached by MBRs of different sizes and that two different routes to chaos are present, depending on the MBR size. In particular, a quasiperiodic doubling for MBRs with diameters below 600 µm and an abrupt transition for bigger MBRs. The mechanical oscillations were observed as from the transmitted optical field as pure sinusoids, modulated sinusoids due to the presence of higher harmonics and decaying ripples for the case of larger MBRs. We also demonstrated that MBRs can transfer chaos from a strong pump WGM to a very weak probe WGM through the mechanical motion and that the two signals follow the same route to chaos. In prospective, this feature could be exploited as a sensing mechanism for an MBR photonic platform capable of various detection mechanisms [25]. On a more general note, the results of our experiment on MBRs demonstrate that chaotic oscillations are a shared feature of WGMRs, which is not limited to specific geometries such as spheres and tori.

Acknowledgments

X. Roselló-Mechó acknowledges FPI programme del Ministerio de Economía y Competitividad, Project TEC2016-76664-C2-1-R. M. Delgado Pinar acknowledges the short term scientific mobility program of COST ACTION MP1401 "Aflaser". S.Soria and G. Frigenti acknowledge the funding from CNR bilateral project RFBR-CNR.

X. Roselló-Mechó performed the optomechanical measurements at high pump powers, and designed the figures of the paper. D. Farnesi fabricated the sub-millimetrical bubbles and performed the measurements at low pump power. G. Frigenti fabricated the MBR up to 460 um and together with M.

Delgado Pinar performed some measurements of characterization and chaos transition. G. Frigenti also designed some of the figures of the paper. F. Ratto performed the COMSOL simulations. G. Nunzi Conti designed the experimental setup and supervised the experiment. S. Soria analysed the data and wrote the manuscript. M. V. Andres collaborated in the discussion of the results. All authors collaborated in the correction of the manuscript.

The authors declare that they do not have competing interests.

References

[1] S. Berneschi, D. Farnesi, F. Cosi, G. N. Conti, S. Pelli, G. C. Righini, S. Soria, High q silica microbubble resonators fabricated by arc discharge, Opt. Lett. 36 (17) (2011) 3521–3523. doi:10.1364/OL.36.003521.
URL http://ol.osa.org/abstract.cfm?URI=ol-36-17-3521

[2] M. Sumetsky, Y. Dulashko, R. S. Windeler, Optical microbubble resonator, Opt. Lett. 35 (7) (2010) 898–900. doi:10.1364/OL.35.000898.
URL http://ol.osa.org/abstract.cfm?URI=ol-35-7-898

[3] G. C. Righini, S. Soria, Biosensing by wgm microspherical resonators, Sensors 16 (6) (2016). doi:10.3390/s16060905.
URL https://www.mdpi.com/1424-8220/16/6/905

[4] Y. Yang, Y. Ooka, R. M. Thompson, J. M. Ward, S. Nic Chormaic, Degenerate four-wave mixing in a silica hollow bottle-like microresonator, Opt. Lett. 41 (3) (2016) 575–578. doi:10.1364/OL.41.000575.
URL http://ol.osa.org/abstract.cfm?URI=ol-41-3-575

[5] Y. Yang, X. Jiang, S. Kasumie, G. Zhao, L. Xu, J. M. Ward, L. Yang, S. Nic Chormaic, Four-wave mixing parametric oscillation and frequency comb generation at visible wavelengths in a silica microbubble resonator, Opt. Lett. 41 (22) (2016) 5266–5269. doi:10.1364/OL.41.005266.
URL http://ol.osa.org/abstract.cfm?URI=ol-41-22-5266

[6] D. Farnesi, G. Righini, G. Nunzi Conti, S. Soria, Efficient frequency generation in phoxonic cavities based on hollow whispering gallery mode resonators, Scientific Reports 7 (2017). doi:10.1038/srep44198.
URL https://doi.org/10.1038/srep44198

[7] D. Farnesi, A. Barucci, G. C. Righini, G. N. Conti, S. Soria, Generation of hyper-parametric oscillations in silica microbubbles, Opt. Lett. 40 (2015) 4508–4511. doi:10.1364/OL.40.004508.
URL http://ol.osa.org/abstract.cfm?URI=ol-40-19-4508

[8] G. Bahl, K. H. Kim, W. Lee, J. Liu, X. Fan, T. Carmon, Brillouin cavity optomechanics with microfluidic devices, Nature Communications 4 (2013). doi:10.1038/ncomms2994.
URL https://doi.org/10.1038/ncomms2994

[9] X. Roselló Mechó, Whispering gallery modes: Advanced photonic applications, Ph.D. thesis, University of Valencia (2019).
URL https://www.educacion.gob.es/teseo/imprimirFicheroTesis.do?idFichero=Wge8

[10] T. J. Kippenberg, H. Rokhsari, T. Carmon, A. Scherer, K. J. Vahala, Analysis of radiation-pressure induced mechanical oscillation of an optical microcavity, Phys. Rev. Lett. 95 (2005) 033901. doi:10.1103/PhysRevLett.95.033901.
URL https://link.aps.org/doi/10.1103/PhysRevLett.95.033901

[11] V. Braginsky, S. Strigin, S. Vyatchanin, Parametric oscillatory instability in fabry–perot interferometer, Physics Letters A 287 (5) (2001) 331–338. doi:https://doi.org/10.1016/S0375-9601(01)00510-2.
URL https://www.sciencedirect.com/science/article/pii/S0375960101005102

[12] M. Aspelmeyer, T. J. Kippenberg, F. Marquardt, Cavity optomechanics, Rev. Mod. Phys. 86 (2014) 1391–1452. doi:10.1103/RevModPhys.86.1391.
URL https://link.aps.org/doi/10.1103/RevModPhys.86.1391

[13] T. J. Kippenberg, K. J. Vahala, Cavity optomechanics: Back-action at the mesoscale, Science 321 (5893) (2008) 1172–1176. doi:10.1126/science.1156032.
URL https://science.sciencemag.org/content/321/5893/1172

[14] T. Kippenberg, K. Vahala, Cavity opto-mechanics, Opt. Express 15 (25) (2007) 17172–17205. doi:10.1364/OE.15.017172.
URL http://www.opticsexpress.org/abstract.cfm?URI=oe-15-25-17172

[15] H. Rokhsari, T. J. Kippenberg, T. Carmon, K. J. Vahala, Radiation-pressure-driven micro-mechanical oscillator, Opt. Express 13 (14)

(2005) 5293–5301. doi:10.1364/OPEX.13.005293.
URL http://www.opticsexpress.org/abstract.cfm?URI=oe-13-14-5293

[16] T. Carmon, H. Rokhsari, L. Yang, T. J. Kippenberg, K. J. Vahala, Temporal behavior of radiation-pressure-induced vibrations of an optical microcavity phonon mode, Phys. Rev. Lett. 94 (2005) 223902. doi:10.1103/PhysRevLett.94.223902.
URL https://link.aps.org/doi/10.1103/PhysRevLett.94.223902

[17] T. Carmon, M. C. Cross, K. J. Vahala, Chaotic quivering of micron-scaled on-chip resonators excited by centrifugal optical pressure, Phys. Rev. Lett. 98 (2007) 167203. doi:10.1103/PhysRevLett.98.167203.
URL https://link.aps.org/doi/10.1103/PhysRevLett.98.167203

[18] M. Asano, Y. Takeuchi, W. Chen, S. K. Özdemir, R. Ikuta, N. Imoto, L. Yang, T. Yamamoto, Observation of optomechanical coupling in a microbottle resonator, Laser & Photonics Reviews 10 (4) (2016) 603–611. doi:https://doi.org/10.1002/lpor.201500243.
URL https://onlinelibrary.wiley.com/doi/abs/10.1002/lpor.201500243

[19] X. Roselló-Mechó, D. Farnesi, G. Frigenti, A. Barucci, A. Fernández-Bienes, T. García-Fernández, F. Ratto, M. Delgado-Pinar, M. V. Andrés, G. Nunzi Conti, S. Soria, Parametrical optomechanical oscillations in phoxonic whispering gallery mode resonators, Scientific Reports 9 (2019). doi:10.1038/s41598-019-43271-x.
URL https://doi.org/10.1038/s41598-019-43271-x

[20] R. Suzuki, T. Kato, T. Kobatake, T. Tanabe, Suppression of optomechanical parametric oscillation in a toroid microcavity assisted by a kerr comb, Opt. Express 25 (23) (2017) 28806–28816. doi:10.1364/OE.25.028806.
URL http://www.opticsexpress.org/abstract.cfm?URI=oe-25-23-28806

[21] F. Monifi, J. Zhang, S. K. Özdemir, B. Peng, Y.-x. Liu, F. Bo, F. Nori, L. Yang, Optomechanically induced stochastic resonance and chaos transfer between optical fields, Nature Photonics 10 (2016) 399–405. doi:10.1038/nphoton.2016.73.
URL https://doi.org/10.1038/nphoton.2016.73

[22] A. Cosci, F. Quercioli, D. Farnesi, S. Berneschi, A. Giannetti, F. Cosi, A. Barucci, G. N. Conti, G. Righini, S. Pelli, Confocal reflectance microscopy for determination of microbubble resonator thickness, Opt. Express 23 (13) (2015) 16693–16701. doi:10.1364/OE.23.016693.
URL http://www.opticsexpress.org/abstract.cfm?URI=oe-23-13-16693

[23] T. Carmon, L. Yang, K. J. Vahala, Dynamical thermal behavior and thermal self-stability of microcavities, Opt. Express 12 (20) (2004) 4742–4750. doi:10.1364/OPEX.12.004742.
URL http://www.opticsexpress.org/abstract.cfm?URI=oe-12-20-4742

[24] L. Bakemeier, A. Alvermann, H. Fehske, Route to chaos in optomechanics, Phys. Rev. Lett. 114 (2015) 013601. doi:10.1103/PhysRevLett.114.013601.
URL https://link.aps.org/doi/10.1103/PhysRevLett.114.013601

[25] G. Frigenti, L. Cavigli, A. Fernández-Bienes, F. Ratto, S. Centi, T. García-Fernández, G. Nunzi Conti, S. Soria, Resonant microbubble as a microfluidic stage for all-optical photoacoustic sensing, Phys. Rev. Applied 12 (2019) 014062. doi:10.1103/PhysRevApplied.12.014062.
URL https://link.aps.org/doi/10.1103/PhysRevApplied.12.014062